ADVANCED FUNCTIONAL MATERIALS
www.afm-journal.de

www.MaterialsViews.com

Fully Solution-Processed Conductive Films Based on Colloidal Copper Selenide Nanosheets for Flexible Electronics

*Sergey Vikulov, Francesco Di Stasio, Luca Ceseracciu, Pearl L. Saldanha, Alice Scarpellini, Zhiya Dang, Roman Krahne, Liberato Manna, and Vladimir Lesnyak**

A novel colloidal synthesis of copper selenide nanosheets (NSs) with lateral dimensions of up to 3 µm is developed. This material is used for the fabrication of flexible conductive films prepared via simple drop-casting of the NS dispersions without any additional treatment. The electrical performance of these coatings is benchmarked against copper selenide spherical nanocrystals (SNCs) in order to demonstrate the advantage of 2D morphology of the NSs for flexible electronics. In this contest, $Cu_{2-x}Se$ SNC films exhibit higher conductivity but lower reproducibility due to the formation of cracks leading to discontinuous films. Furthermore, the electrical properties of the films deposited on different flexible substrates following their bending, stretching and folding are studied. A comparison of $Cu_{2-x}Se$ SNC and CuSe NS films reveals an increased stability of the CuSe NS films under mechanical stress applied to the samples and their improved long-term stability in air.

1. Introduction

Flexible electronics is a rapidly growing field, which promises the development of a variety of novel commercial products as displays, solar cells, and biomedical sensors that can be embedded in clothes and other everyday items.[1] Typically, flexible electronic devices take advantage of the mechanical properties of conventional plastic materials such as polystyrene or polymethylmethacrylate and semiconductor properties of conjugated polymers.[2] Many polymers indeed exhibit high-flexibility, and therefore organic materials are dominant in flexible electronics. However, only a few conductive polymers are available, with poly(3,4-ethylenedioxythiophene)-poly(styrenesulfonate) (PEDOT:PSS), the most commonly used, thus restricting fabrication techniques, material choices, and applications.[3] This imposes strict limitations on the design of flexible devices, for example greatly reducing the available work function values for electrodes. Moreover, conjugated polymers generally exhibit a relatively low charge carrier mobility and low overall chemical stability,[2c,4] as compared to inorganic semiconductor compounds. Widening the range of conductive and flexible materials that can be processed with low-cost solution-based techniques, such as drop-casting, spin-coating, spray-deposition, etc., can be achieved by employing colloidal inorganic nanomaterials in combination with commercially available plastics. In this case, since substrate and coating are often mechanically mismatched, the mechanical resistance and preservation of functionality when the device withstands the expected deformation must be guaranteed.[5]

Colloidal nanocrystals (NCs) represent an alternative material that can be processed at low temperature into conducting or semiconducting thin films for high performance flexible electronics.[4,6] In this approach, one of the key advantages is that optical and electronic properties of NCs can be tuned by controlling their size, shape, and composition.[1a,7] The NCs in the form of concentrated solutions or dispersions (so-called inks), both in polar and nonpolar solvents, can easily be processed into thin-films on a wide range of substrates.[8] Nevertheless, the electrical performance (i.e., carrier mobility) of NC-based solids is still limited due to a large number of interfaces between particles in solids and poor contacts between adjacent particles, which are usually capped by insulating organic ligands employed in the synthesis. Great progress in NC-based electronics has recently been achieved through the introduction of small inorganic capping ligands, which significantly reduce the distance between particles and thus dramatically improve communication between NCs within the solid.[9] Nevertheless, this type of ligand modification requires the employment of polar organic solvents with high dielectric constants such as formamide and its derivatives. These are all high boiling

S. Vikulov, Dr. F. Di Stasio, P. L. Saldanha, A. Scarpellini, Dr. Z. Dang, Prof. R. Krahne, Prof. L. Manna, Dr. V. Lesnyak
Department of Nanochemistry
Istituto Italiano di Tecnologia
via Morego 30, 16163 Genoa, Italy
E-mail: vladimir.lesnyak@iit.it, vladimir.lesnyak@chemie.tu-dresden.de

Dr. L. Ceseracciu
Smart Materials
Istituto Italiano di Tecnologia
via Morego 30, 16163 Genoa, Italy

Dr. V. Lesnyak
Physical Chemistry
TU Dresden
Bergstr. 66b, 01062 Dresden, Germany

Note: The copyright line of this article was amended on June 7, 2016

DOI: 10.1002/adfm.201600124

compounds that hamper further processing of NCs, and lead to the formation of "bulk-like" systems that cannot be used for the fabrication of flexible films. Alternatively, by using 1D nanowire- or nanotube-inks, one can greatly reduce the number of the grain boundaries within the solid. However, thin-films obtained from these 1D nanostructures usually have a limited surface coverage, with restricted current delivering ability or require sophisticated assembly approaches.[10] This obstacle can be overcome by employing 2D semiconductor nanostructures with a thickness much smaller than their lateral dimensions. These are a valuable alternative to ultrathin layers deposited on substrates by various techniques like atomic layer deposition, chemical (physical) vapour deposition, and molecular beam epitaxy.[11]

Among inorganic semiconductors, metal chalcogenides have been in focus of intensive research owing to their promise in optoelectronic applications.[1a,7a] Main members of groups II-VI, IV-VI, and III-V metal chalcogenides contain either toxic (Cd, Pb, Hg) or rare (In, Ga) elements. Therefore, during the last years, the limelight has been shifted toward their low toxic and abundant alternatives such as copper chalcogenides. Among them, copper selenide represents one of the most interesting materials since it is a superionic conductor that shows p-type conductivity due to copper vacancies within its crystal lattice.[8b,12] Copper selenide can be prepared in a variety of stoichiometric and non-stoichiometric crystal phases, such as cubic berzelianite (Cu_2Se or $Cu_{7.16}Se_4$), hexagonal klockmannite (CuSe or $Cu_{0.87}Se$), tetragonal umangite (Cu_3Se_2), and orthorhombic athabascaite (Cu_5Se_4 or CuSe); as well as in different morphologies like spherical nanoparticles,[12,13] nanocubes,[14] nanorods,[15] nanowires,[16] and hierarchical nanostructures.[17] Furthermore, a few examples of 2D copper selenide in the form of nanoplates and nanosheets (NSs) have recently been reported.[8b,15,18]

In view of the discussion outlined above, in this work we developed a novel synthesis of klockmannite CuSe NSs with average lateral sizes exceeding 1 μm and thickness of ≈5 nm. These sheets were processed into thin films by simple drop-casting of their concentrated dispersions onto different substrates, including flexible plastics and paper at room temperature without any additional heat treatment and ligand modification. Electrical characterization revealed that these films exhibited conductivities of up to 645 $S \cdot m^{-1}$. Furthermore, using recently developed heavily doped $Cu_{2-x}Se$ spherical NCs (SNCs) for comparison,[13d] we demonstrated the advantages of the 2D morphology of the CuSe NSs for retention of their conductivity after bending, stretching, and folding (see **Figure 1**). In these experiments, the conductivity of the CuSe NS films was restored to the initial values after releasing the mechanical stress, whereas the conductivity of $Cu_{2-x}Se$ SNC-based films irreversibly dropped after releasing the stress applied to flexible substrates. Moreover, the CuSe NS films demonstrated higher resistance toward aging compared to the $Cu_{2-x}Se$ SNCs.

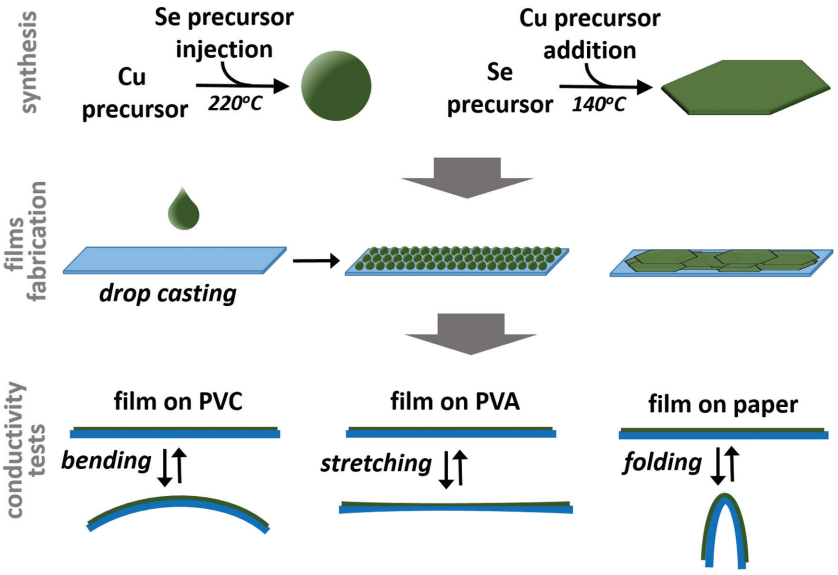

Figure 1. A general scheme of the experiments performed: syntheses of copper selenide SNCs and NSs with their subsequent processing into the films by drop casting on various substrates (polyvinylchloride (PVC), polyvinyl alcohol (PVA), paper), followed by testing their conductivity upon bending, stretching and folding.

2. Results and Discussion

2.1. Synthesis and Characterization of the Copper Selenide Nanosheets

The synthesis of CuSe NSs developed in this work is based on our previous reports on $Cu_{2-x}Se_yS_{1-y}$ nanoplates[18c] and $Cu_{2-x}Se$ SNCs.[13d] The main difference with the previously reported procedure is in the way of mixing Cu- and Se-precursors: addition of the Cu-precursor to the Se-precursor heated to 140 °C, as opposed to the rapid injection of Se-precursor into the Cu- one used previously (see the scheme in Figure 1). In this case, the copper precursor reacts with an excess of the selenium precursor yielding klockmannite CuSe instead of berzelianite $Cu_{2-x}Se$ crystal structure. As a byproduct of the reaction we observed a small fraction (less than 5%) of SNCs.

The obtained NSs exhibited a hexagonal or truncated triangular shape and a broad distribution of lateral sizes from 0.2 to 3 μm, with a constant thickness of ≈5 nm, as shown by transmission electron microscopy (TEM) imaging (see **Figure 2**a,b). When attempting to measure their thickness by atomic force microscopy, we always observed stacks of several NSs due to their strong tendency to aggregation on a wafer. High resolution TEM (HRTEM) analysis revealed that these hexagonal, triangular NSs and small nanoplates have hexagonal crystal phase with a = 3.948 Å and c = 17.285 Å. Figure 2 c,d displays the HRTEM image of a region of a single hexagonal NS and corresponding fast Fourier transform (FFT) pattern. The hexagonal NSs were oriented in zone axis [001], while the triangular NSs and nanoplates were oriented in other zone axes. At a higher temperature (160–180 °C), the NSs fused together during the synthesis forming larger and thicker irregularly shaped sheets (see Figure S1 in the Supporting Information). The Cu/Se ratio in the sheets was 1 ± 0.05 according to elemental analysis

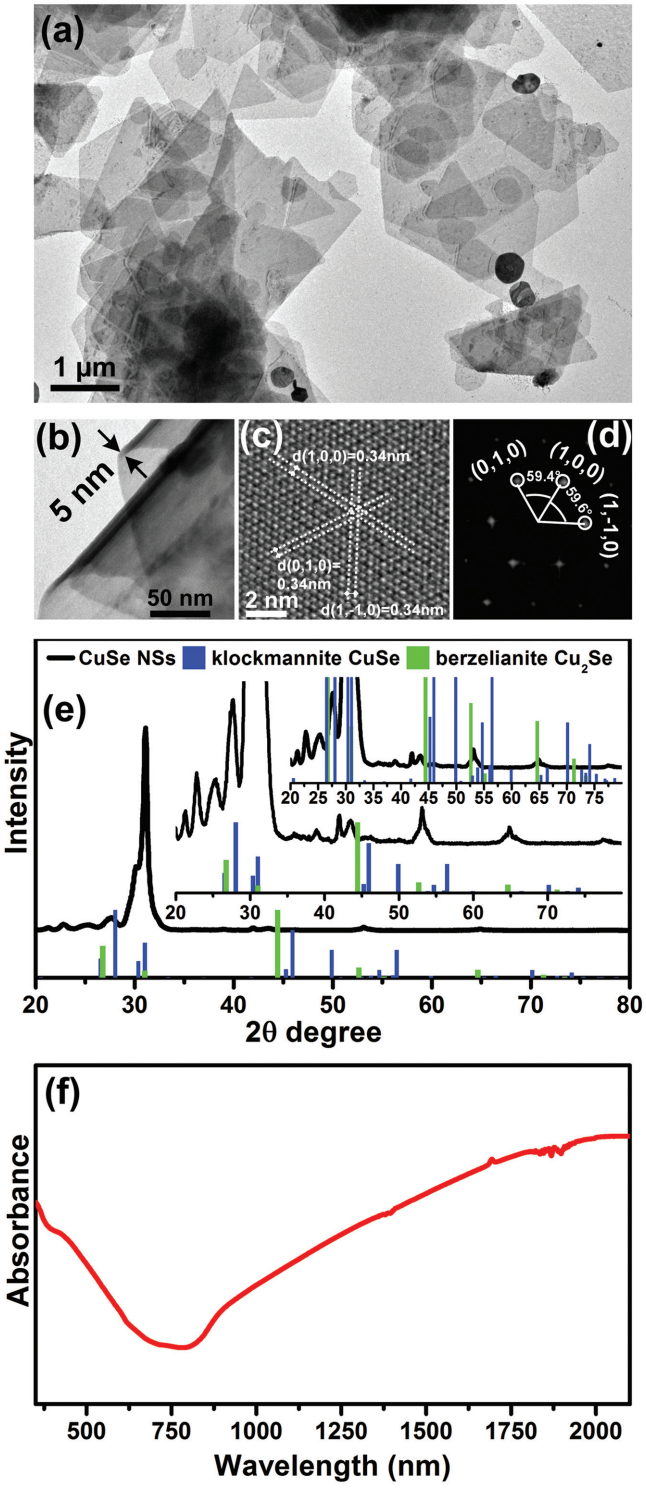

Figure 2. TEM images of CuSe NSs: a) overview and b) magnified side-view of fragments of two-folded NSs showing their thickness of ≈ 5 nm. c) HRTEM image of a section of a hexagonal NS oriented in the [001] zone axis with d) corresponding FFT pattern. e) XRD pattern of CuSe NSs. The experimental pattern is compared to database powder diffraction files of hexagonal CuSe klockmannite (PDF card #03-065-3562) and cubic Cu_2Se berzelianite (PDF card #01-071-4325). f) Optical absorption spectrum of CuSe NSs dispersed in tetrachloroethylene.

performed on several samples from different batches. In solution the NSs tended to form aggregates, similar to what reported by Wu et al.,[18d] a large part of which precipitated upon storage. Nevertheless, the dispersions formed in toluene or chloroform were sufficiently stable to be processed into thin films.

Powder X-ray diffraction (XRD) analysis of CuSe NSs demonstrated that the dominating crystal structure of the sample was hexagonal CuSe klockmannite (PDF card #03-065-3562), in accord with the HRTEM results, although, as can be seen in Figure 2e, some peaks of the pattern can be assigned also to the cubic CuSe berzelianite (PDF card #01-071-4325) crystallographic phase, which was present as small particles in the sample. The intensity of the diffraction peak at 31° is higher than the others suggesting that CuSe NSs are oriented preferentially horizontally, parallel to the substrate.[8a] The optical absorption spectrum of the CuSe NSs presented in Figure 2f exhibits a broad band extending from ≈750 nm further to the NIR region, which is similar to the spectra of recently reported CuS[19] and CuSe[8b] NSs. This kind of absorption in copper chalcogenide nanostructures is attributed to a localized surface plasmon resonance generated by the collective oscillation of holes.[20] Its broadening and shift to longer wavelengths are caused by a significant in-plane delocalization of charge carriers, similar to anisotropic $Cu_{2-x}S$ nanodisks with a broad localized surface plasmon resonance.[21] The broadening of the plasmon band and its shift to lower energies has also been observed previously by our group in films of $Cu_{2-x}Se$ SNCs,[12] where charge carriers were delocalized within adjacent nanoparticles brought in close contact.

2.2. Films Preparation and Their Electrical Characterization

As-synthesized CuSe NSs, without any additional treatment and surface modification, were processed into thin films by drop-casting their chloroform dispersions onto different substrates, such as glass-slides, flexible plastics, and paper at room temperature. A relatively slow evaporation of the solvent (≈40 min) led to homogeneous films without macro- and microscopical cracks, as demonstrated by surface profile analysis (see Figure S2, Supporting Information) and scanning electron microscopy (SEM) imaging (Figure S3, Supporting Information). In these films, NSs preferentially lay horizontally (i.e., parallel to the substrate surface) and randomly overlap with adjacent sheets forming a continuous layer (see **Figure 3**). Owing to their thinness, CuSe NSs are flexible and easily adapt to the relief (see Figure S3, Supporting Information). At the same time, as seen in the cross-sectional SEM image shown in Figure 3b, there are some voids in the film due to imperfect arrangement of some NSs and their bending and folding. The SNC films appeared continuous with close packed nanoparticles in SEM images, while profilometric analysis over length scales of some millimeters revealed typical film thickness values of several micrometers with fluctuations up to 1 μm (Figure S2, Supporting Information).

The electrical properties of the films were investigated using a four contact van der Pauw method.[22] The main preparation conditions of the films and their properties are summarized in Table S1 (Supporting Information). Based on the

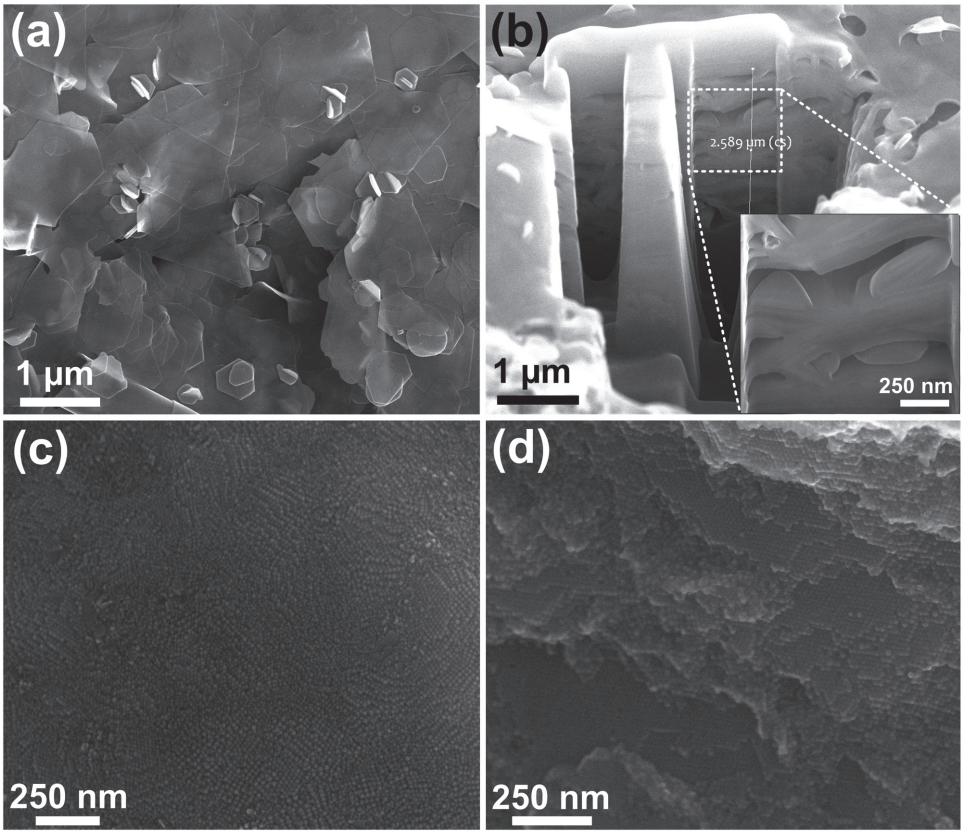

Figure 3. SEM images of a,b) CuSe NSs and c,d) $Cu_{2-x}Se$ SNCs films: a,c) top view, b) cross section of a film made by ion milling, d) side view showing how the nanoparticles are organized in layers within the film.

measurements of a series of different samples, the average conductivity of NS films was 535 $S \cdot m^{-1}$ (median 522 $S \cdot m^{-1}$). It should be noted that we report conductivity values measured on macro-sized samples (2.5 cm × 2.5 cm), which allow us to neglect local nano- and microdefects that play an important role on micropatterned substrates. Our data, in particular, the linear dependence of the current on the voltage (see **Figure 4**a), resemble the metallic (ohmic) behavior of CuSe NS films, similar to the results of Liu et al.[8b] The $Cu_{2-x}Se$ SNCs films had an average conductivity of 2500 $S \cdot m^{-1}$ (median 1730 $S \cdot m^{-1}$), more than four times that of CuSe NS films owing to the presence of a high density of copper vacancies in the SNCs ($x \approx 0.6$),[13d] which in turn increased the number of available holes associated with these vacancies. Nevertheless, a large surface roughness and a possible imperfect packing of these small particles with spherical shape under the employed experimental conditions gave rise to cracks and inhomogeneity in the films, thus inducing a large spread in conductivity values (see Table S1, Supporting Information).

After storage of the samples in air for ≈ 9 months, we repeated the electrical measurements and observed a drop in conductivity of 22% for $Cu_{2-x}Se$ SNCs films, while no deterioration was noticed in the case of the CuSe NS films. The conductivity values measured in this work are much higher than those reported previously on films of $Cu_{2-x}Se$ NCs, in which the NCs were coated either with oleylamine/oleic acid molecules (10^{-9} $S \cdot cm^{-1}$) or with mercaptopropionic acid (10^{-6} $S \cdot cm^{-1}$).[23] This can be attributed to a much higher value of x, i.e. much larger number of copper vacancies in the particles resulting in their high degenerately doping levels. Large differences in conductivity of SNCs may be caused by a partial oxidation of the material exposed to air during film fabrication and measurements, leading to a change of the number of copper vacancies which in turn significantly affects their electronic properties, as demonstrated by the group of Prieto, by the oxidation of initially stoichiometric Cu_2Se NC films.[24] Here we note that although these two materials (CuSe NSs and $Cu_{2-x}Se$ SNCs) have different structures, they are both efficient conductors and thus their comparison focuses mainly on their morphology.

2.2.1. Bending Tests: Films on Polyvinylchloride

In order to demonstrate advantages of the 2D morphology of the NSs, we performed bending, stretching, and folding tests of the films deposited on flexible plastic and paper substrates. The deformations applied during tests on polymer substrates were small compared to the sample size to remain in the elastic regime of the substrate, allowing it to return to original conditions when the stress was released. As a sample for comparison we used $Cu_{2-x}Se$ SNC films. Both films of NSs and SNCs were macroscopically uniform and continuous. Since the curvature of the substrates upon three points bending is variable along

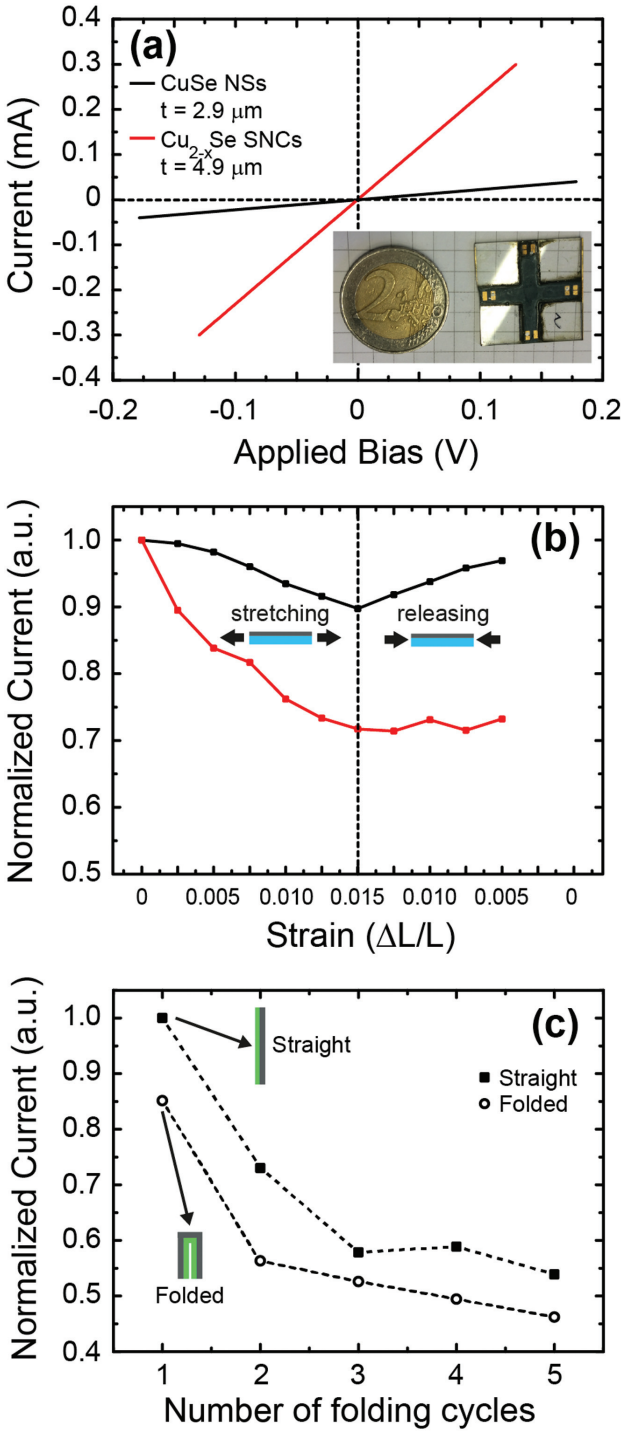

Figure 4. a) Typical *I–V* curve recorded from films of CuSe NSs (average thickness = 2.9 μm, black solid line) on a soda-lime glass, and $Cu_{2-x}Se$ SNCs (average thickness = 4.9 μm, red solid line, color coding is the same for all panels). Inset: photo of a typical "greek cross" sample used for the van der Pauw measurement, compared in size with a 2€ coin. b) Performance of stretchable conductive films on PVA substrate fabricated with CuSe NSs and $Cu_{2-x}Se$ SNCs. The curves are the calculated average values of three different tests per material. The residual deformation upon strain release is attributed to viscous deformation localized at the clamping areas. c) Electrical performance of a CuSe NS film-on-paper upon five cycles of folding-straightening.

the sample length, it is convenient to associate the current recorded at each step with the maximum value, which is reached at the central pin and can be calculated from classic beam theory by Equation (1)

$$\varepsilon = \frac{6t\delta}{L^2} \tag{1}$$

where t is the film thickness, δ is the applied vertical displacement, and L is the distance between outer supports. Such relationship is shown in the plot in Figure S4a (Supporting Information) for both NS and SNC films. As seen from the graph, both NSs- and SNCs-based samples show a loss of current with increasing curvature due to the strain occurring in the film. However, when releasing the displacement, the current in NS films recovered almost completely to its previous value, while in the SNC films the current did not recover to its original state. The conductivity in NS films was reversible upon deformation due to the film morphology consisting of overlapping sheets that enable shifts without formation of cracks. On the other hand, the SNC films underwent irreversible conductivity loss upon external strain, most probably due to a formation of cracks or shear-induced delamination.

2.2.2. Stretching Tests: Films on Polyvinyl Alcohol

Similar results were obtained in the stretching tests, where the NSs and SNCs films deposited onto flexible PVA substrates were strained by applying tension to one of the film ends keeping the other one fixed (see Figure 4b). This time the deformation occurred along the whole substrate. The maximum applied strain (0.015) was chosen from the stress versus strain curve of bare PVA film (Figure S5, Supporting Information), to ensure that the deformation remains in the elastic regime, although the polymer showed viscous deformation from the beginning of the test, visible in the nonlinear response, and therefore strain recovery upon unloading was not complete. As expected, the conductivity of both samples decreased with increased stretching (by 13% for NSs and 38% for SNCs on average). After releasing the tension, the conductivity of the NS films was completely restored to the prestress values, while the SNC films underwent an irreversible loss in conductivity. These results represent a quasistatic analysis of the change of material properties during deformation that are useful for dimensioning the device to guarantee functionality upon in service deformation, rather than a fatigue test, that would be useful to characterize the material's reliability after many bending cycles.[8a] We show that the loss of conductivity of CuSe NS-based films is low and reversible upon realistic stretching and bending conditions in flexible electronic applications. Considering, indeed, the final application in flexible devices, we can calculate the maximal curvature (minimal radius) for a given value of the substrate thickness t, neglecting the much thinner film, using Equation (2)

$$R = \frac{t}{2\varepsilon} \tag{2}$$

Typical values of substrate thickness for flexible electronics are in the 0.05–0.2 mm range.[5] For such values our films would withstand curvature radii of about 1.7 to 7 mm, in agreement with results presented in other works.[25] The sliding mechanism that enables the NS films to recover their conductivity could allow for even much larger values of strain. Therefore, we tested one sample up to 5% of relative elongation and found a linear dependence of current until as much as 3% strain (Figure S4b, Supporting Information), which suggests that the sliding mechanism can hold within this deformation range.

2.2.3. Folding Tests: Films on Paper

As a further test to evaluate the performance of our conductive copper selenide films for application in flexible electronics, we prepared films on a cleanroom type paper (films-on-paper) and measured their resistance under harsh folding conditions. The test was carried out by acquiring the *I–V* curve of films-on-paper while straight and after their folding along the long axis (see Figure S6, Supporting Information). The measured resistance values of all tested CuSe NS films-on-paper were well below 1 kΩ. Figure 4c demonstrates the behaviour of the electrical current of a CuSe NS film-on-paper (initial resistance of 293.3 Ω) in straight and folded configurations for several folding cycles. In the graph, we show the worst performing sample, to emphasize the highest drop in conductivity induced by folding that we observed. The strongest reduction in current (about 15%) was observed after the first folding, in subsequent cycles the relative reduction gradually decreased and the current stabilized at about half of its initial value, resulting in a resistance of 640 Ω of the paper strip. We tested three samples under five cycles of folding, and on average, the CuSe NS films on the paper strips exhibited an initial resistance of around 290 Ω (see Table S2, Supporting Information). After five folding cycles, there was an average current loss of 22.5%. The paper strips always showed a lower resistance in the straight configuration compared to the folded one. All films remained conductive under folding and after the initial cycles their resistance stabilized at values below 1 kΩ. We emphasize that films-on-paper fabricated with SNCs via drop-casting did not show any conductivity, presumably due to a poor contact between the particles which could percolate deep inside the fibrous structure of the paper, once again demonstrating the advantage of the 2D shape of the NSs.

3. Conclusion

We have developed a novel colloidal synthesis of klockmannite CuSe hexagonal nanosheets with lateral sizes larger than 1 µm and thickness of around 5 nm. These 2D structures are easily dispersible in organic solvents and thus can be processed via drop-casting on various substrates without any thermal or chemical treatment. The resulting films showed ohmic behavior, with a conductivity of several hundreds of $S \cdot m^{-1}$ that is maintained for several months under air. The morphology of the nanosheet films with overlapping contacts between the individual sheets resulted in an advantageous behavior on flexible substrates, manifested by an almost complete recovery of their conductivity after the application of a mechanical stress such as bending and stretching. Similar treatment of $Cu_{2-x}Se$ spherical nanoparticle-based samples led to irreversible loss of their conductivity that was in the order of 20%–30%. Furthermore, the nanosheets enabled the deposition of conductive films on paper that remained conductive under folding, with losses significantly lower than one order of magnitude after several folding cycles. These features make the CuSe nanosheets suitable candidates for printable electronics on flexible substrates (e.g., in medical implantation devices) or for a possible use in stress sensors.

4. Experimental Section

Materials: Copper(II) acetylacetonate ($Cu(acac)_2$, 97%), 1-dodecanethiol (DDT, ≥98%), oleylamine (OlAm, 70%), tetrachloroethylene (TCE, ≥99%), and poly(vinyl alcohol) (PVA, M_w 31000-50000) were purchased from Sigma-Aldrich; anhydrous chloroform, methanol, and toluene were purchased from Carlo Erba reagents; and selenium powder (Se, 99.99%) was purchased from STREM Chemicals. All chemicals were used as received without further purification.

Synthesis of CuSe NSs: It was performed using a standard Schlenk-line technique by mixing Cu- and Se-precursors at 140 °C. For the Cu-precursor 1.97 g (5 mmol) of $Cu(acac)_2$ was dissolved in 6 mL DDT and 12 mL OlAm in a three-neck round-bottom flask by degassing the mixture under stirring at 60 °C for ≈1 h (pressure ≈10^{-2} Torr) and subsequent heating up to 140 °C under nitrogen. $Cu(acac)_2$ was completely dissolved forming a clear yellow-orange solution. The hot mixture was loaded into a glass syringe with a 14 gauge needle. Note that, after cooling, the Cu-precursor solidifies forming a viscous slurry, therefore a thick needle should be used for its following addition to the Se-precursor. The Se-precursor was prepared similarly to ref. [26]: 0.4 g of Se powder (5 mmol) was mixed with 4 mL of DDT and 8 mL of OlAm and degassed under stirring at room temperature or at moderate heating up to 30-40 °C for ≈1 h (pressure ≈10^{-2} Torr). Afterward, the flask was filled with nitrogen and heated up to 140 °C, where 12 mL of Cu-precursor (prepared as described above) were added using a syringe pump with a flow rate of 6 mL min^{-1} and vigorous stirring, leading to a color change from brown to greenish-brown with metallic luster. The reaction mixture was kept at 140 °C for 8 min and then cooled to room temperature. The CuSe NSs were separated by centrifugation of the resulting mixture, and washed 2-3 times by dispersion in 3 mL of chloroform and subsequent centrifugation. Finally, the NSs were dispersed in 3 mL of chloroform.

Synthesis of $Cu_{2-x}Se$ SNCs: This was performed according to a recipe from ref. [13d].

Elemental Analysis: Inductively coupled plasma optical emission spectroscopy (ICP-OES) analysis was performed with an iCAP 6000 spectrometer (ThermoScientific) to quantify the copper and selenium content in the samples. For sample preparation, typically a 10–25 µL volume of NSs or SNCs dispersion was digested in 2.5 mL of aqua regia (HCl/HNO_3 = 3/1 (v/v)) overnight with subsequent dilution up to 25 mL with Milli-Q water in a plastic flask. Finally, the solution was filtered through a 0.45 µm PTFE syringe filter.

Transmission Electron Microscopy (TEM): Samples were prepared by drop-casting diluted NCs or NSs dispersions onto a carbon coated 200 mesh copper grids for conventional TEM imaging. TEM images were recorded on a JEOL JEM 1011 microscope equipped with a thermionic gun operating at 100 kV.

High Resolution TEM (HRTEM): Samples were prepared by drop-casting diluted NSs onto an ultrathin holy carbon film supported by a lacey carbon film on a 400 mesh copper grids for HRTEM imaging. HRTEM was performed on a JEOL JEM-2200FS microscope equipped with a Schottky emitter operated at 200 kV, a CEOS spherical aberration corrector of the objective lens, and an in-column Omega filter.

Scanning Electron Microscopy (SEM): Samples were prepared by deposition of ≈10 µL of NCs or NSs dispersion in chloroform on a silicon substrate with subsequent evaporation of the solvent. Cross sectioning and imaging of the film was carried out with a Nova 600 NanoLab microscope (FEI), equipped with a field emission gun for scanning electron imaging and a focused ion beam of gallium ions for milling. A preliminary in situ platinum coating was performed to protect the sample's surface from the ion milling. The sectioning process was done in two steps, which consisted of ion current milling (working at 30 kV and 7.7 pA) followed by a cleaning step of the section. Imaging, before and after the cross sectioning, was done with the secondary electrons detector at an acceleration voltage of 20 kV (0.4 nA of emission current).

Powder X-Ray Diffraction (XRD) Analysis: XRD patterns were recorded with a Rigaku SmartLab 9 kW diffractometer. The X-ray source was operated at 40 kV and 150 mA. The diffractometer was equipped with a Cu source and a Göbel mirror to obtain a parallel beam and to suppress Cu Kβ radiation (1.392 Å). To acquire data, a 2-theta/omega scan geometry was used. The samples were prepared by drop casting concentrated NSs dispersions onto a zero background silicon substrate. The PDXL software of Rigaku was used for phase identification.

Optical Absorption Spectra of NSs dispersed in TCE were measured on a Varian Cary 5000 UV–vis–NIR spectrophotometer.

Electrical Characterization: Films for electrical characterization were prepared via drop casting of CuSe NS dispersions in chloroform (550 µL) and solutions of $Cu_{2-x}Se$ SNCs in a mixture of chloroform and toluene (450 µL) on glass slides previously templated with a polyimide tape to obtain a "greek cross" shaped film of defined size of 2.5 × 2.5 cm. Evaporation of the solvents was carried out in air for ≈40 min. After drying, a second layer of copper selenide NSs and SNCs was cast using the same volumes of the colloids, resulting in a dark grey homogeneous film. Following the film preparation, 1 × 1 mm gold pads were evaporated at the end of the "greek cross" arms as electrical contacts. The conductivity of these films was measured using the van der Pauw method.[22] Electrical measurements were carried out employing a SUSS microtec probe station PM5, a Keithley 2612 sourcemeter and an Agilent 3440 digital multimeter. All measurements were performed in air, using the Keithley 2612 to apply a current on two arms on the "greek cross" shaped films, and the voltage drop was measured at the opposite arms of the film using the Agilent digital multimeter.

For the bending tests, films on flexible polyvinylchloride (PVC) substrate were prepared by drop-casting the chloroform suspensions of NSs and SNCs with concentrations of 0.012 mg mL^{-1} and 0.015 mg mL^{-1}, respectively. The suitability for application of flexible electronics was evaluated by flexural tests on a Q800 DMA testing machine (TA Instruments). Samples were cut in 20 × 35 mm rectangles with 0.45 mm thickness and mounted on a three-point bending clamp with a span length of 20 mm. After mounting, the films were connected to a sourcemeter (Keithley 2612) for electrical characterization. The initial current was measured with an applied bias of 2 V, then a displacement δ of the center pin was applied in steps of 500 µm with the rate of 1 mm min^{-1} up to 2500 µm. After the bending, the film was released step-wise upon the same conditions, at each step the current was measured upon the same applied bias.

For the stretching tests, we first fabricated a PVA film as a substrate for deposition of the NSs and SNCs as follows. 0.1 mg of PVA was dissolved in 10 mL of water with three drops of HCl, and left for 3 days at 90 °C under stirring. 500 µL of the resulting solution were drop-cast on 18 × 18 mm PTFE substrates and left drying overnight forming a 0.03 mm thick transparent film. Drop-casting of 300 µL of nanoparticles dispersion in chloroform (0.022 mg mL^{-1} for NSs and 0.050 mg mL^{-1} for SNCs) was then carried out on the PVA surface to obtain the conductive film. Dry films were then peeled off from the PTFE substrate and cut in rectangles of 18 × 5 mm. Then they were placed on the testing machine equipped with a uniaxial tension clamp (clamps distance ≈ 10 mm) and connected to the current measurement setup described above. The initial current was measured with an applied bias of 0.1 V, then the samples were elongated by steps of 25 µm with the rate of 50 µm min^{-1} until 150 µm, corresponding to a strain of about 1.5%, then released with the same stepwise procedure to evaluate whether the variation of conductivity induced by stretching was reversible. An additional test was carried out up to a larger strain, namely 5%, to evaluate the electrical response to a broader extent, although in this case the substrate reached full plastic deformation, therefore it was not possible to evaluate the current recovery upon load release.

For the folding tests, copper selenide NS and SNC films-on-paper were prepared via drop-casting 300 µL of a CuSe NSs chloroform suspension (0.009 mg mL^{-1}) on a polymer saturated cleanroom paper (Texwipe TexWrite 22 Cleanroom Bond Paper from Fischer Scientific). The obtained films were left to dry and then were cut in 4 × 1 cm stripes. Films-on-paper using SNCs were prepared using the same technique but they did not show any electrical conductivity. Films-on-paper were then connected with two clamps to a Keithley 2612 sourcemeter. The resistivity measurements were performed by applying a voltage of 1 V, and with the help of a support to obtain the two different configurations: straight and folded (Figure S5 in the Supporting Information).

Profilometry Analysis of the Films: Film thickness and surface profiles were measured employing a Dektak profilometer. Thickness values reported in Table S1 (Supporting Information) are the calculated average from five different measurements carried out on different areas of the film (the value was calculated from the average surface height reported by the instrument for a line trace of 600 µm). The surface profiles reported in Figure S2 (Supporting Information) were obtained from the films used for the electrical measurements on glass.

Supporting Information

Supporting Information is available from the Wiley Online Library or from the author.

Acknowledgements

S.V. and F.D.S. contributed equally to this work. The authors thank Sergio Marras for the help in XRD measurements. V.L. acknowledges the support by a Marie Curie Intra European Fellowship within the 7th European Community Framework Programme (FP7/2007-2013) under the grant agreement no. 301100 (project "LOTOCON"). S.V. and L.M. acknowledge the support by the 7th European Community Framework Programme (FP7/2007-2013) under the grant agreement no. 614897 (ERC Consolidator Grant "TRANS-NANO").

Received: January 8, 2016
Revised: February 26, 2016
Published online: April 18, 2016

[1] a) Z. Liu, J. Xu, D. Chen, G. Shen, *Chem. Soc. Rev.* **2015**, *44*, 161; b) D.-H. Kim, N. Lu, R. Ghaffari, J. A. Rogers, *NPG Asia Mater.* **2012**, *4*, e15.
[2] a) Y.-H. Kim, J.-S. Heo, T.-H. Kim, S. Park, M.-H. Yoon, J. Kim, M. S. Oh, G.-R. Yi, Y.-Y. Noh, S. K. Park, *Nature* **2012**, *489*, 128; b) Q. Cao, H.-S. Kim, N. Pimparkar, J. P. Kulkarni, C. Wang, M. Shim, K. Roy, M. A. Alam, J. A. Rogers, *Nature* **2008**, *454*, 495; c) S. R. Forrest, *Nature* **2004**, *428*, 911.
[3] S. Ju, A. Facchetti, Y. Xuan, J. Liu, F. Ishikawa, P. Ye, C. Zhou, T. J. Marks, D. B. Janes, *Nat. Nanotechnol.* **2007**, *2*, 378.
[4] C. Wang, H. Dong, W. Hu, Y. Liu, D. Zhu, *Chem. Rev.* **2012**, *112*, 2208.
[5] J. Lewis, *Mater. Today* **2006**, *9*, 38.
[6] S. R. Thomas, P. Pattanasattayavong, T. D. Anthopoulos, *Chem. Soc. Rev.* **2013**, *42*, 6910.
[7] a) D. V. Talapin, J.-S. Lee, M. V. Kovalenko, E. V. Shevchenko, *Chem. Rev.* **2010**, *110*, 389; b) H. Zhang, *ACS Nano* **2015**, *9*, 9451; c) H. Li,

J. Wu, Z. Yin, H. Zhang, *Acc. Chem. Res.* **2014**, *47*, 1067; d) X.-J. Wu, X. Huang, X. Qi, H. Li, B. Li, H. Zhang, *Angew. Chem. Int. Ed.* **2014**, *53*, 8929.

[8] a) Z. Lin, Y. Chen, A. Yin, Q. He, X. Huang, Y. Xu, Y. Liu, X. Zhong, Y. Huang, X. Duan, *Nano Lett.* **2014**, *14*, 6547; b) Y.-Q. Liu, F.-X. Wang, Y. Xiao, H.-D. Peng, H.-J. Zhong, Z.-H. Liu, G.-B. Pan, *Sci. Rep.* **2014**, *4*, 5998.

[9] a) M. V. Kovalenko, M. Scheele, D. V. Talapin, *Science* **2009**, *324*, 1417; b) D. S. Dolzhnikov, H. Zhang, J. Jang, J. S. Son, M. G. Panthani, T. Shibata, S. Chattopadhyay, D. V. Talapin, *Science* **2015**, *347*, 425; c) A. Nag, M. V. Kovalenko, J.-S. Lee, W. Liu, B. Spokoyny, D. V. Talapin, *J. Am. Chem. Soc.* **2011**, *133*, 10612; d) H. Zhang, J. Jang, W. Liu, D. V. Talapin, *ACS Nano* **2014**, *8*, 7359.

[10] Y. Huang, X. F. Duan, Q. Q. Wei, C. M. Lieber, *Science* **2001**, *291*, 630.

[11] a) C. Bouet, M. D. Tessier, S. Ithurria, B. Mahler, B. Nadal, B. Dubertret, *Chem. Mater.* **2013**, *25*, 1262; b) E. Lhuillier, S. Pedetti, S. Ithurria, B. Nadal, H. Heuclin, B. Dubertret, *Acc. Chem. Res.* **2015**, *48*, 22.

[12] S. Deka, A. Genovese, Y. Zhang, K. Miszta, G. Bertoni, R. Krahne, C. Giannini, L. Manna, *J. Am. Chem. Soc.* **2010**, *132*, 8912.

[13] a) D. Dorfs, T. Härtling, K. Miszta, N. C. Bigall, M. R. Kim, A. Genovese, A. Falqui, M. Povia, L. Manna, *J. Am. Chem. Soc.* **2011**, *133*, 11175; b) C. M. Hessel, V. P. Pattani, M. Rasch, M. G. Panthani, B. Koo, J. W. Tunnell, B. A. Korgel, *Nano Lett.* **2011**, *11*, 2560; c) X. Liu, W.-C. Law, M. Jeon, X. Wang, M. Liu, C. Kim, P. N. Prasad, M. T. Swihart, *Adv. Healthcare Mater.* **2013**, *2*, 952; d) V. Lesnyak, R. Brescia, G. C. Messina, L. Manna, *J. Am. Chem. Soc.* **2015**, *137*, 9315.

[14] W. Li, R. Zamani, M. Ibáñez, D. Cadavid, A. Shavel, J. R. Morante, J. Arbiol, A. Cabot, *J. Am. Chem. Soc.* **2013**, *135*, 4664.

[15] G. Xiao, J. Ning, Z. Liu, Y. Sui, Y. Wang, Q. Dong, W. Tian, B. Liu, G. Zou, B. Zou, *CrystEngComm* **2012**, *14*, 2139.

[16] X. Chen, Z. Li, J. Yang, Q. Sun, S. Dou, *J. Colloid Interface Sci.* **2015**, *442*, 140.

[17] Y. Li, S. L. Luo, L. X. Yang, C. B. Liu, Y. Chen, D. S. Meng, *Electrochim. Acta* **2012**, *83*, 394.

[18] a) Z. Deng, M. Mansuripur, A. J. Muscat, *J. Mater. Chem.* **2009**, *19*, 6201; b) J. Choi, N. Kang, H. Y. Yang, H. J. Kim, S. U. Son, *Chem. Mater.* **2010**, *22*, 3586; c) V. Lesnyak, C. George, A. Genovese, M. Prato, A. Casu, S. Ayyappan, A. Scarpellini, L. Manna, *ACS Nano* **2014**, *8*, 8407; d) X.-J. Wu, X. Huang, J. Liu, H. Li, J. Yang, B. Li, W. Huang, H. Zhang, *Angew. Chem. Int. Ed.* **2014**, *53*, 5083.

[19] Y. Du, Z. Yin, J. Zhu, X. Huang, X.-J. Wu, Z. Zeng, Q. Yan, H. Zhang, *Nat. Commun.* **2012**, *3*, 1177.

[20] a) Y. Zhao, H. Pan, Y. Lou, X. Qiu, J. Zhu, C. Burda, *J. Am. Chem. Soc.* **2009**, *131*, 4253; b) J. M. Luther, P. K. Jain, T. Ewers, A. P. Alivisatos, *Nat. Mater.* **2011**, *10*, 361; c) A. Comin, L. Manna, *Chem. Soc. Rev.* **2014**, *43*, 3957; d) Y. Zhao, C. Burda, *Energy Environ. Sci.* **2012**, *5*, 5564; e) X. Liu, M. T. Swihart, *Chem. Soc. Rev.* **2014**, *43*, 3908; f) J. A. Faucheaux, A. L. D. Stanton, P. K. Jain, *J. Phys. Chem. Lett.* **2014**, *5*, 976.

[21] a) S.-W. Hsu, K. On, A. R. Tao, *J. Am. Chem. Soc.* **2011**, *133*, 19072; b) S.-W. Hsu, W. Bryks, A. R. Tao, *Chem. Mater.* **2012**, *24*, 3765.

[22] L. J. van der Pauw, *Philips Res. Repts.* **1958**, *13*, 1.

[23] X. Liu, X. Wang, B. Zhou, W.-C. Law, A. N. Cartwright, M. T. Swihart, *Adv. Funct. Mater.* **2013**, *23*, 1256.

[24] S. C. Riha, D. C. Johnson, A. L. Prieto, *J. Am. Chem. Soc.* **2011**, *133*, 1383.

[25] a) Q. Cao, S. H. Hur, Z. T. Zhu, Y. G. Sun, C. J. Wang, M. A. Meitl, M. Shim, J. A. Rogers, *Adv. Mater.* **2006**, *18*, 304; b) Z. Liu, J. Li, F. Yan, *Adv. Mater.* **2013**, *25*, 4296.

[26] Y. Liu, D. Yao, L. Shen, H. Zhang, X. Zhang, B. Yang, *J. Am. Chem. Soc.* **2012**, *134*, 7207.